Phosphorene Degradation: Visualization and Quantification of Nanoscale Phase Evolution by Scanning Transmission X-ray Microscopy

*Weihan Li[1, 2, #], Zhiqiang Wang [2, #], Feipeng Zhao[1, #], Minsi Li[1,2], Xuejie Gao[1,2], Yang Zhao,[1] Jian Wang,[3] Jigang Zhou,[3] Yongfeng Hu,[3] Qunfeng Xiao,[3] Xiaoyu Cui[3], Mohammad Javad Eslamibidgoli[4, †], Michael. H. Eikerling[4, †], Ruying Li [1], Frank Brandys[5], Ranjith Divigalpitiya[5], Tsun-Kong Sham [2, *], Xueliang Sun[1,*]*

[1]*Department of Mechanical and Materials Engineering, University of Western Ontario, London, Ontario, N6A 5B9, Canada*
[2] *Department of Chemistry and Soochow-Western Centre for Synchrotron Radiation Research, University of Western Ontario, London, Ontario, N6A 5B7, Canada*
[3] *Canadian Light Source, 44 Innovation Boulevard, Saskatoon, Saskatchewan, S7N 2V3, Canada*
[4] *Department of Chemistry, Simon Fraser University, 8888 University Drive, Burnaby, V5A 1S6, BC, Canada*
[5]*3M Canada Company, 1840 Oxford Street East, London, Ontario, N5V 3R6, Canada*

*Corresponding Author: Xueliang Sun, Tel: +1-519-661-2111 Ext 87759; Tsun-Kong Sham, Tel: Tel: +1-519-661-2111 Ext 86341;

E-mail address: xsun9@uwo.ca (X. Sun); tsham@uwo.ca (T.K. Sham)

[#]These authors contributed equally to this work.

[†] These authors contributed in the theoretical study of this work.

ABSTRACT

Phosphorene, single- or few-layered black phosphorus, has been rediscovered as a promising two-dimensional material owing to its unique optical, thermal, and electrical properties with potential applications in optoelectronics, nanoelectronics and energy storage. However, rapid degradation under ambient condition highly limits the practical applications of phosphorene. Solving the degradation problem demands understanding of the oxidization process. We for the first time apply synchrotron-based X-ray photoelectron spectroscopy (XPS), X-ray absorption near-edge structure (XANES) and scanning transmission X-ray microscopy (STXM) for the nanoscale chemical imaging

of phosphorene degradation. Through these methods, we have identified chemical details of the morphological effect and clarified thickness and proximity effects, which control the oxidization process. Furthermore, the entire oxidization process of phosphorene has also been studied by *in-situ* XPS and XANES, showing the step-by-step oxidization process under the ambient condition. Theoretical calculations at the density functional theory level support experimental findings. This detailed study provides a better understanding of phosphorene degradation and is valuable for the development of phosphorene-based materials.

KEYWORDS:
Phosphorene, degradation, STXM, XANES, XPS

Introduction

Recently, phosphorene, single- or multi-layered black phosphorus (BP) has been rediscovered as a two-dimensional (2D) electronic material and has received intensive attention in research since its first isolation in 2014, showing an orthorhombic structure with puckered double layers.[1-3] The renaissance of phosphorene was driven by a unique set of properties, including the tunable direct band gap (from 0.3 eV of bulk BP to 2.0 eV of the monolayer structure), and high carrier mobility (up to 1,000 $cm^2V^{-1}s^{-1}$ observed experimentally and up to 10,000-26,000 $cm^2V^{-1}s^{-1}$ predicted by theory).[3-7] In addition, the anisotropic in-plane properties of phosphorene, such as optical, thermal, and electrical properties, make it promising for applications in optoelectronics, nanoelectronics and energy storage.[8-12] However, the rapid degradation of phosphorene under the ambient condition impedes its practical applications.[13, 14]

The degradation process is related to two main effects, environmental effect (e.g. light, oxygen and water) and morphological effect (e.g. thickness and oxidized regions in the vicinity); in the ambient, degradation occurs from several hours to days.[15, 16] Upon exposure to light, oxygen defects are initially formed which then react with water to form a mixture of oxides and phosphoric acid.[17-19] While the thickness (i.e. number of layers) of the material determines its band structure and oxidization mechanism, the

existing regions already oxidized will affect the oxidation kinetics of the unoxidized region in the vicinity, expanding the local oxide layer thickness and expediting the degradation process.[14, 20] Several groups have applied optical microscopy,[15, 21] atomic force microscopy,[16, 18, 22] and Raman spectroscopy[17] to track morphology changes during phosphorene degradation under different environments, showing the gradual transformation from a smooth surface to a rough surface with growing oxides protrusions and bubbles.

To understand the chemical reaction behind the morphology change, X-ray photoelectron spectroscopy (XPS),[23, 24] electron energy loss spectroscopy (EELS),[22] anion-exchange chromatography (AEC),[25] and nuclear magnetic resonance (NMR) studies[26] have been carried out to track the variation of valence states and chemical compositions. Furthermore, quantum mechanical calculations based on density functional theory (DFT) have been performed to develop an atomistic understanding of the processes leading to oxide formation and phosphorene degradation.[19, 27] In addition to environmental effects, the morphological effect has also been investigated using AFM, scanning Raman microscopy (SRM) and Infrared scattering scanning near-field microscopy (IR s-SNOM).[16, 20, 28] In one study, it was found that the thinner regions of phosphorene show higher degradation rate (i.e. thickness effect), tracked by the AFM and SRM, while the oxidized phosphorene accelerates the degradation of adjacent regions (i.e. neighboring effect), as also suggested by the phenomenological modeling of IR s-SNOM result. Nevertheless, these three reports of morphological effect study mainly focused on the variation of morphology and few reports presented a clear and detailed picture from a chemical point of view.[17] In another study, R. Martel et. al used transmission electron microscopy (TEM) to track the thickness information by high-angle annular dark field (HAADF) contrast and the oxidation states by EELS images, presenting the thickness effect on phosphorene degradation.[17] However, the energy resolution of EELS images is limited, showing inadequate chemical sensitivity to distinguish different oxidation states.[29] Considering the previous works, the main challenge to realize detailed analysis and to obtain a clear conclusion of morphology

effect is the ability to image the local morphology and chemical states at nanoscale resolution.

As sensitive methods to characterize oxidation states, synchrotron-based XPS and X-ray absorption fine structure (XAFS), especially X-ray absorption near-edge spectroscopy (XANES) are two of the most precise techniques to clarify the chemical states and the coordination chemistry.[30-32] In addition, absolute thickness information of samples can be calculated based on the edge jump, if XANES is conducted on an individual nanosheet through the transmission mode.[33, 34] Therefore, XANES is sensitive to the thickness-dependent chemical changes of phosphorene. However, the beam size commonly used for XANES is in the order of millimeters, which is not suitable for the spatial scale of phosphorene (around tens to hundreds of nanometers). To further improve the spatial resolution of XANES, synchrotron-based scanning transmission X-ray microscopy (STXM), which combining an undulator source and zone plate optics is further considered to realize high spatial resolution, enabling nanoscale chemical imaging and absolute thickness measurements.[31, 35]

In this work, we applied synchrotron-based STXM at the nanoscale resolution for the very first time (~30 nm in this case), together with *in-situ* synchrotron-based XPS (high energy resolution, high photon intensity and high cross-section due to photon energy tunability) and XANES at the P K-edge to study the degraded phosphorene under the ambient condition.[36] Taking advantages of the morphology sensitivity of X-ray microscopy, and the thickness and chemical sensitivity of XPS and XANES, the oxidation states of several regions corresponding to the thickness and the interaction between adjacent regions have been probed. By chemical mapping of degraded phosphorene at the nanoscale, the thickness effect and proximity effect have been obtained, clarifying the morphological effect on phosphorene degradation. The thinner regions are easier to be oxidized and the already oxidized phosphorene tend to aggravate the degradation of the adjacent regions. In addition, based on the *in-situ* XPS and XANES study of the phosphorene degradation, the oxidization process of phosphorene in air is revealed. Fresh phosphorene is initially oxidized to P(III) and then subsequently oxidized to P(V) and phosphorene oxidation starts from the surface and

then spreads to the inside parts through the analysis of the averaged chemical states of phosphorene.

Results and discussion

Phosphorene under investigation was prepared by liquid exfoliation of bulk BP in *N*-Methyl-2-pyrrolidone (NMP) via tip-sonication.[37] To avoid degradation of phosphorene during the liquid exfoliation process, all procedures were carried out in an inert atmosphere (See Experimental section for details). **Figure S1** (See Supporting Information) displays the transmission electron microscopy (TEM) and high-resolution TEM (HRTEM) images of the phosphorene thus prepared. The phosphorene shows ultrathin nanosheet morphology and a typical crystalline structure with a lattice spacing of 0.22 nm corresponding to the (014) crystal plane. The lattice structure of phosphorene indicates no obvious degradation, in accordance with the scanning electron microscopy (SEM) of phosphorene (See Supporting Information, **Figure S2**). As shown in Figure S2, the phosphorene nanosheets range from around several hundred nanometers to several micrometers in size. To obtain the thickness information of the phosphorene nanosheet, atomic force microscopy (AFM) has been carried out and the phosphorene ranges from 3 nm to 14 nm in thickness (See Supporting Information, **Figure S3**A), corresponding to the blue-shift and decreased intensity of Raman peaks (See Supporting Information, **Figure S4**).[15, 38]

To understand the degradation process of phosphorene under ambient condition, *in-situ* synchrotron-based XPS and XANES studies have been carried out to track the oxidation states of degraded phosphorene during the process (See Experimental section for details). Synchrotron-based XPS spectra of fresh phosphorene (fresh-Pn) and degraded phosphorene for 1h and 5h (D-Pn-1h and D-Pn-5h) are shown in **Figure 1A.** Owing to the excitation photon energy of 240.00 eV, the probing depth is just around 1 nm (escape depth of the P 2p photoelectrons), realizing high surface sensitivity of around a couple of black phosphorus atomic layers. In the case of fresh-Pn (Figure 1B), it shows the typical P 2p XPS spectra with one characteristic doublet belonging to the P $2p_{3/2}$ and $2p_{1/2}$ orbitals with the peak positions of 130.00 and 130.86 eV, respectively.

The spin-orbit splitting of around 0.86 eV is an atomic characteristic of phosphorus atoms.[23] No other XPS peaks at higher binding energy means only phosphorus-phosphorus bonds in fresh-Pn without any oxidization. After degradation for 1 h under ambient condition, XPS peaks belonging to two oxidation states, P(III) and P(V) are found in D-Pn-1h, consistent with previous results (Figure 1C).[25, 26] After another 4 h degradation, D-Pn-5h shows similar oxidation peaks with increased intensity, suggesting more extensive oxidation after longer degradation time (Figure 1D), which is further confirmed by *in-situ* P K-edge XANES study conducted at the fluorescence yield (FLY) mode. As shown in Figure 1E, *in-situ* XANES of phosphorene degradation was carried out focusing the X-ray beam on the same area of phosphorene degraded for up to 1200 h. Fresh-Pn shows typical XANES spectra with the white line at around 2145.2 eV, which is related to the electron transition from P 1s orbital to the unoccupied electronic states of P 3p character.[39] After exposure to ambient atmosphere for over 5 h, the degraded Pn (D-Pn) shows one peak belonging to fresh-Pn and two peaks centered at 2151.4 and 2153.3 eV belonging to two higher oxidation states. Compared with the reference spectra of P_2O_5 and phosphates (See Supporting Information, **Figure S5**), the oxidation states for the D-Pn are a mixture of P(0) and P(III) & P(V).[40] While the intensity of P(0) peaks gradually decreases with increasing degradation time, P(III) and P(V) peaks display an opposite tendency, meaning that longer degradation time leads to more extensive oxidation and to higher oxidation states.

To quantitatively analyze the phosphorene degradation process, *in-situ* XPS and XANES result was fitted to find out the phase evolution (See Supporting Information, **Figure S6**).[41-43] As shown in Figure 1F, the combination fitting result of XPS spectra shows the phase evolution at the surface (~1 nm), the content of P(III) and P(V) increases with the degradation time and the P(V) content (i.e. 6.4 % and 11.5% at 1 and 5 h, respectively) is constantly higher than that of P(III) (i.e. 5.91 % and 10.8% at 1 and 5 h, respectively). Similarly, the linear combination fitting (LCF) result of XANES spectra (Figure 1G) shows the mixture of P(III) and P(V) oxidation states in the XPS or XANES spectra suggest that both transformation processes from P(0) to P(III) and from P(III) to P(V) take place simultaneously.[43] However, the XANES spectra show

different conclusion owing to the bulk sensitivity (several micro meters) of the FLY mode at the beginning of phosphorene degradation, lower P(III) and P(V) phase percentage (2.7 % and 2.5 %, respectively) after 5h degradation. Additionally, the lower content of P(V) than P(III) is opposite from the XPS result. That means that the oxidation and degradation of phosphorene start from the surface and then spread to the bulk. The different intensity ratio of P(III) to P(V) at the surface and in the bulk suggests that phosphorene degradation is a two-step process. When phosphorene is exposed to ambient condition, P(III) is firstly formed, which is chemically unstable and then transformed to P(V). At the surface, formed P(III) is easier to be further oxidized by oxygen. However, it is more difficult for the oxygen to go through the surface and then oxidize the formed P(III) in the bulk, leading to lower content of P(V) inside. After the initial degradation, the formation of P(III) also faces the oxygen-penetration problem. The content of P(V) starts to be higher than P(III). Based on the combination result after different degradation time, the phase evolution rate of P(0), P(III), and P(V) is calculated and shown in Figure 1H. The three phases show the similar rate evolution tendency, which goes down at the beginning and then goes up at the end. That means initially formed oxidation surface layer blocks the contact between oxygen and phosphorene part and gradually-increasing oxidation layer lowers down the degradation rate. However, the continuous degradation process finally leads to collapse of crystal structure of entire phosphorene sheets, which promotes the degradation process together with the transformation from hydrophobic phosphorene to hydrophilic oxidized phosphorene.[22] At the end of phosphorene, P(V) can be expected to be the highest oxidation state after complete degradation, consistent with previous reports.[14, 17, 19, 26]

To further understand the oxidation mechanism of phosphorene, VASP package[44] was used to carry out DFT calculations at the dispersion corrected PBE-D3/zero level[45]. To simulate the black phosphorus surface, calculations under periodic boundary condition were performed on a two-layer BP slab. A vacuum space of 30 Å was added between repeated slab layers to minimize interactions between them. The surface

formation energy was calculated as a function of oxygen coverage which varies between zero and one monolayer (ML),

$$\gamma^{BPO} = \frac{1}{2A}\left(E_{O/BP} - NE_{BP/bulk} - \frac{n}{2}E_{O2}\right), \qquad (1)$$

where A is the unit-cell surface area, $E_{O/BP}$ the total energy of the oxygen-covered surface, $E_{BP/bulk}$ the calculated energy of BP in the bulk unit-cell, and E_{O2} the energy of molecular oxygen in gas phase; N is the ratio of the number of P atoms in slab configuration to that in the bulk unit-cell, and n is the number of adsorbed O atoms.

The calculated surface formation energies are shown in **Figure 2**. For coverage below 0.5 ML, the most preferred adsorption site for O is the on-top dangling position (as shown in (a) and (b) in Figure 2). On the other hand, for coverage above 0.5 ML, adsorption on the dangling position is not energetically favored (as shown in (c) and e) in Figure 2), and the surface undergoes structural reconstruction to form PO_3 and PO_4 groups. Upon this surface reconstruction, P atoms are displaced from their original position at the surface and become coordinated with 3 or 4 oxygen atoms (as shown in (d) and (f) in Figure 2 and See Supporting Information, **Figure S11**). The geometry of surface PO_3 groups is similar to that of phosphorus trioxide (P_4O_6), in which phosphorus atoms are coordinated with 3 O atoms. Similarly, the geometry of the PO_4 groups formed at higher oxygen coverage is analogues to the structure of phosphorus pentoxide (P_4O_{10}) in which the phosphorus atoms are bound by a tetrahedron of oxygen atoms. Thus, as also compared to the formation energies of P_4O_6 and P_4O_{10} clusters in Figure 2, theoretical results confirm the experimental findings of the two-step oxidation process of phosphorene that will eventually lead to the formation of P_2O_5. Furthermore, P_4O_6 and P_4O_{10} are susceptible to moisture absorption and will be transformed to corresponding phosphoric acid (i.e. H_3PO_3 and H_3PO_4). Our DFT results, thus, confirm the observation based on *in-situ* synchrotron-based XPS and XANES study, that the oxidation mechanism of phosphorene under ambient condition proceeds as a two-step process. Fresh phosphorene is first oxidized to P(III) and further transformed to P(V) after prolonged degradation. And the oxidation starts from the surface and then spread to the inside parts. Coordinates of the main structures were provided in the Supporting

Information along with the surface energies calculated for various other terminations of O^{ad} on black phosphorus.[27]

Having revealed the chemical reaction during phosphorene degradation process, we study the morphology effect during phosphorene degradation process using STXM, by studying the exact specimen on a TEM grid that had been investigated with TEM. As shown in **Figure 3A**, STXM is conducted by focusing the beam with a Fresnel zone plate to a small spot and rasterizing over the phosphorene samples. It has strict thickness requirements for thickness measurements comparable to that of TEM. After collecting the X-ray microscopy images at a series of photon energies known as energy stacks (often as small steps, in tenth of an eV for examsple across the absorption edge of a specific element), the XANES spectra of each pixel can be obtained.[31] Additionally, the absolute thickness of phosphorene at each pixel can be acquired by fitting the XANES spectra with the quantitatively scaled reference spectra of fresh phosphorene (See Supporting Information, **Figure S7A**). The phosphorene thickness map determined at the P K-edge is displayed in Figure 3B, presenting the nanosheet morphology, in accordance with the TEM and SEM images (Figures S1 & S2). Based on the thickness distribution map, eight regions with different thickness (from 10 nm to 700 nm) have been selected to acquire the P K-edge XANES spectra, showing similar features compared with fresh BP and indicating no obvious oxidation peaks (Figure 3C). While the absorption peak with the white line at around 2145.2 eV is consistent with XANES spectrum of fresh-Pn, the broader white line is ascribed to the lower instrument energy resolution at the edge of energy range for the SXTM beamline.[39]

Then, the phosphorene was left in the ambient condition and degraded for a long time (30 days) to obtain oxidation information of prolong exposure, denoted as D-Pn-30d, and to study the degradation mechanism of phosphorene. As shown in Figure S6A (See Supporting Information), the nano-XANES spectrum acquired from the entire overall region of D-Pn-30d shows similar features compared with the XANES spectrum of D-Pn-700h shown in the above *in-situ* XANES study. The broader peaks are also ascribed to the lower energy resolution for the SXTM beamline as noted above. However, the oxidation states in D-Pn-30d can be also interpreted as a mixture of P(0),

P(III), and P(V). To further resolve the detailed composition of mixed oxidation states, XANES spectrum fitting was conducted as shown in Figure S6B (See Supporting Information).[41-43] Based on the XANES spectral fitting and composition fitting, the phase ratio of P(0), P(III), and P(V) is determined to be 6:3:1.

To quantitatively analyze the morphological effect during the degradation process of phosphorene, the thickness maps determined at the P K-edge of P(0), P(III) and P(V) are essential and they are presented in **Figure 4A ~ 4C** by conducting P K-edge stack of D-Pn-30d fitting with the quantitatively scaled reference spectra of phosphorene and phosphoric acid (See Supporting Information, Figure S7A, S7B and S7C). Based on the thickness maps and XANES spectra, one quasi-quantitative intensity distribution map of P(0) and P(III&V) in D-Pn-30d is displayed in Figure 4D, which uses the broad peak corresponding to the mixture of P(III) and P(V) as the reference oxidation mixture spectra (See supporting Information, Figure S6B and S7D). Compared with the AFM study of phosphorene degradation (See Supporting Information, Figure S3B), which just presents the morphology change without chemical information, STXM can provide detailed chemical imaging of degraded phosphorene. Three regions of interest (ROIs) have been selected in Figures 5D, marked as a, b, and c, corresponding to the lowest, medium and highest degree of oxidizations, respectively. The exact degree of oxidization of each ROI can be directly presented through the XANES spectra. As presented in the **Figure S8** (See Supporting Information), the XANES spectra of ROIs a, b, and c show gradual transformation to higher oxidation states with the increasing intensity of P(III&V) and decreasing intensity of P(0). Furthermore, ROIs a and c are dominated by P(0) and P(V) peaks, respectively, indicating that while ROI a just starts to be oxidized, the phosphorus in ROI c has been fully oxidized.

To get a better understanding of the morphological effect on the degradation process of phosphorene, ROIs with different thicknesses and surrounding environments of D-Pn-30d have been selected (i.e. ROIs a, b, and c), as shown in **Figure 5A**. Based on the thickness maps in Figure 4A ~ 4C, the thickness information of phosphorene and P(III) and P(V) oxides at the ROIs is listed in **Table S1** (See Supporting Information), showing the thickness of a fresh phosphorene at these ROIs before degradation (a: 9.8

nm; b: 8.5 nm; c: 4.7 nm). Then the chemical state of these ROIs is shown in Figure 5B, displaying a mixture of P(0), P(III), and P(V). Furthermore, the phase percentage of P(0), P(III), and P(V) in there ROIs is shown in the insert of Figure 5B, calculated based on the linear combination fitting (LCF) (See Supporting Information, **Figure S9**). Comparing their ROIs, it is clear that the higher content of P(III) and P(V) is in the thinner phosphorene, meaning higher degree of oxidation. This result should be related to the thickness-dependent band structure, suggesting that the thickness effect plays a significant role on phosphorene degradation under ambient condition.[19]

In addition, based on the thickness variation result shown in Table S1 (See Supporting Information), degraded phosphorene shows increased thickness after the formation of P(III) and P(V) compared with fresh phosphorene, consistent with previous theoretical calculations and experimental results.[14, 20] Moreover, the already oxidized regions are capable of increasing the local layer thickness and even resulting in cracking the crystal structure of neighborhood regions, accelerating the oxidization of phosphorene in theory, concluded as the proximity effect.[14] Up to now, the proximity effect has only been studied by the phenomenological modeling of IR s-SNOM result with no direct chemical information.[20] Based on the STXM result displayed in Figure 5A, four RIOs have been marked with black circles as shown in Figures 6C ~ 6F. Each region marked with the dash line in Figures 6C ~ 6F displays the similar thickness of phosphorene. Based on the thickness effect discussed above, different areas in each region should show similar degree of oxidization. However, through comparing the phase combination images in each region, the areas near the edge, next to the adjacent highly oxidized regions tends to be in higher oxidization states than the center parts away from the highly oxidized regions. This result indicates that the highly oxidized regions would promote the oxidization of the adjacent areas and the neighborhood effect, as shown in the schematic illustration is apparent (Figure 5G). The quantitative analysis result of the proximty effect in several regions is shown in **Figure 6**. Along with the blue arrows marked in Figures 6A, 6D & 6G, a series of gradually varied XANES spectra at the P K-edge is shown in Figures 6B, 6E & 6H. It is apparent from the edge to the center, the intensities of P(III&V) peaks gradually increase while the

P(0) peaks gradually decrease, showing that the already oxidized regions will accelerate the oxidation of adjacent regions. This result is further confirmed by the LCF, as shown in Figure 6C, 6F & 6I, suggesting the obvious neighborhood effect during phosphorene degradation. Additionally, the normalized XANES spectra and LCF result of the overall regions marked in Figures 6A, 6D & 6G are shown in **Figure S10** (See Supporting Information), showing that the thinner regions show higher degree of oxidization compared to the thicker ones.

Based on the above result and discussion, it is clear that the phosphorene degradation under ambient condition is a step-by-step process and starts from the surface to the inside parts. Initially, the thinner region of phosphorene is firstly oxidized under the impact of light and oxygen, which absorbs moisture and transforms to phosphoric acid. Then the already oxidized regions in phosphorene increase the layer thickness and produce defects, accelerating the oxidation of adjacent regions. During the oxidization process, P(III) is firstly formed and then further oxidized to be P(V). With increasing degradation time, the content of P(III) and P(V) increases at the expense of P(0). Regarding the evolution of phosphorene degradation in the sheets, the degradation starts at the surface and the oxygen penetrate through the surface and oxidize the inside parts. The degradation rate decreases after the initial oxidation at the surface due to the block of oxygen penetration by the surface and then increases at the end owing to the collapse of entire crystal structure and hydrophilic properties of phosphorene oxides. At the final degradation stage, phosphorene will be fully transformed to P(V) oxide.

Conclusion

We have for the first time provided a clear nanoscale chemical imaging of the morphology effect during phosphorene degradation under ambient condition using STXM, and macroscopic specimens using *in-situ* synchrotron-based XPS and XANES spectra. The high spatial and chemical resolution of STXM, provides unprecedented morphology information (e.g. thickness and adjacent situation) and reveals the oxidation states of degraded phosphorene at any given region of interest. Through

analyzing the effect of thickness and adjacent regions of degraded phosphorene, the thickness and proximity effects during phosphorene degradation clearly emerge from a chemical perspective: The thinner phosphorene is easier to be oxidized owing to the band structure and the oxidized regions can accelerate the degradation of adjacent regions, which contribute to the phosphorene degradation process, simultaneously. Furthermore, the oxidization process of phosphorene was also studied by *in-situ* XPS and XANES; the results show that fresh phosphorene is firstly oxidized to be P(III) and then further oxidized to be P(V) in short time under the ambient condition. Additionally, the oxidation starts at the surface and then spread to the inside parts, resulting fully oxidized state at last. Thus, a better understanding of the morphology effect during phosphorene degradation has been achieved in this work using a combination of synchrotron-based STXM, XPS, and XANES techniques, which will facilitate the development of phosphorene, especially the protection strategies.

Supporting Information

Additional information and figures.

Acknowledgements

This work was funded by the Nature Sciences and Engineering Research Council of Canada (NSERC), the Canada Research Chair Program, the Canada Foundation for Innovation (CFI), 3M Canada, the Ontario Research Fund, the Canada Light Source (CLS) at the University of Saskatchewan, and the University of Western Ontario. CLS was supported by CFI, NSERC, NRC, CHIR, and the University of Saskatchewan. Minsi Li and Xuejie Gao thank the China Scholarship Council (CSC) for the financial support. Weihan Li, Zhiqiang Wang, Feipeng Zhao, Minsi Li and Xuejie Gao acknowledge the receipt of support from the CLSI Graduate and Post-Doctoral Student Travel Support Program. We also appreciate the help of the beamline scientists of Beamline 9-BM at Advanced Photon Source, Dr. Tianpin Wu and Dr. Lu Ma. We also

thank Prof. Gianluigi Botton, Dr. Hanshuo Liu, and Andrei Carmen in McMaster University for the help and support.

References:

1. P. Bridgman, *Journal of the American Chemical Society*, 1914, **36**, 1344-1363.
2. A. Carvalho, M. Wang, X. Zhu, A. S. Rodin, H. Su and A. H. C. Neto, *Nature Reviews Materials*, 2016, **1**, 16061.
3. L. Li, Y. Yu, G. J. Ye, Q. Ge, X. Ou, H. Wu, D. Feng, X. H. Chen and Y. Zhang, *Nature nanotechnology*, 2014, **9**, 372.
4. X. Ling, H. Wang, S. Huang, F. Xia and M. S. Dresselhaus, *Proceedings of the National Academy of Sciences*, 2015, **112**, 4523-4530.
5. V. Tran, R. Soklaski, Y. Liang and L. Yang, *Physical Review B*, 2014, **89**, 235319.
6. L. Li, J. Kim, C. Jin, G. J. Ye, D. Y. Qiu, H. Felipe, Z. Shi, L. Chen, Z. Zhang and F. Yang, *Nature nanotechnology*, 2017, **12**, 21.
7. J. Qiao, X. Kong, Z.-X. Hu, F. Yang and W. Ji, *Nature communications*, 2014, **5**, 4475.
8. H. Jang, J. D. Wood, C. R. Ryder, M. C. Hersam and D. G. Cahill, *Advanced Materials*, 2015, **27**, 8017-8022.
9. Z. Luo, J. Maassen, Y. Deng, Y. Du, R. P. Garrelts, M. S. Lundstrom, D. Y. Peide and X. Xu, *Nature communications*, 2015, **6**, 8572.
10. F. Xia, H. Wang and Y. Jia, *Nature communications*, 2014, **5**, 4458.
11. R. Fei and L. Yang, *Nano letters*, 2014, **14**, 2884-2889.
12. Y. Xue, Q. Zhang, T. Zhang and L. Fu, *ChemNanoMat*, 2017, **3**, 352-361.
13. A. Ziletti, A. Carvalho, P. Trevisanutto, D. Campbell, D. Coker and A. C. Neto, *Physical Review B*, 2015, **91**, 085407.
14. A. Ziletti, A. Carvalho, D. K. Campbell, D. F. Coker and A. C. Neto, *Physical review letters*, 2015, **114**, 046801.
15. A. Castellanos-Gomez, L. Vicarelli, E. Prada, J. O. Island, K. Narasimha-Acharya, S. I. Blanter, D. J. Groenendijk, M. Buscema, G. A. Steele and J. Alvarez, *2D Materials*, 2014, **1**, 025001.
16. J. O. Island, G. A. Steele, H. S. van der Zant and A. Castellanos-Gomez, *2D Materials*, 2015, **2**, 011002.
17. A. Favron, E. Gaufrès, F. Fossard, A.-L. Phaneuf-L’ Heureux, N. Y. Tang, P. L. Lévesque, A. Loiseau, R. Leonelli, S. Francoeur and R. Martel, *Nature materials*, 2015, **14**, 826.
18. T. Ahmed, S. Balendhran, M. N. Karim, E. L. Mayes, M. R. Field, R. Ramanathan, M. Singh, V. Bansal, S. Sriram and M. Bhaskaran, *npj 2D Materials and Applications*, 2017, **1**, 18.
19. Q. Zhou, Q. Chen, Y. Tong and J. Wang, *Angewandte Chemie International Edition*, 2016, **55**, 11437-11441.
20. S. Gamage, Z. Li, V. S. Yakovlev, C. Lewis, H. Wang, S. B. Cronin and Y. Abate, *Advanced Materials Interfaces*, 2016, **3**, 1600121.

21. J. D. Wood, S. A. Wells, D. Jariwala, K.-S. Chen, E. Cho, V. K. Sangwan, X. Liu, L. J. Lauhon, T. J. Marks and M. C. Hersam, *Nano letters*, 2014, **14**, 6964-6970.
22. Y. Huang, J. Qiao, K. He, S. Bliznakov, E. Sutter, X. Chen, D. Luo, F. Meng, D. Su and J. Decker, *Chemistry of Materials*, 2016, **28**, 8330-8339.
23. M. Edmonds, A. Tadich, A. Carvalho, A. Ziletti, K. O'Donnell, S. Koenig, D. Coker, B. Ozyilmaz, A. C. Neto and M. Fuhrer, *ACS applied materials & interfaces*, 2015, **7**, 14557-14562.
24. W. Luo, D. Y. Zemlyanov, C. A. Milligan, Y. Du, L. Yang, Y. Wu and D. Y. Peide, *Nanotechnology*, 2016, **27**, 434002.
25. T. Zhang, Y. Wan, H. Xie, Y. Mu, P. Du, D. Wang, X. Wu, H. Ji and L. Wan, *Journal of the American Chemical Society*, 2018.
26. Y. Wang, B. Yang, B. Wan, X. Xi, Z. Zeng, E. Liu, G. Wu, Z. Liu and W. Wang, *2D Materials*, 2016, **3**, 035025.
27. M. J. Eslamibidgoli and M. H. Eikerling, *The Journal of Physical Chemistry C*, 2018, **122**, 22366-22373.
28. G. Abellán, S. Wild, V. Lloret, N. Scheuschner, R. Gillen, U. Mundloch, J. Maultzsch, M. Varela, F. Hauke and A. Hirsch, *Journal of the American Chemical Society*, 2017, **139**, 10432-10440.
29. A. E. Goode, A. E. Porter, M. P. Ryan and D. W. McComb, *Nanoscale*, 2015, **7**, 1534-1548.
30. F. Lin, Y. Liu, X. Yu, L. Cheng, A. Singer, O. G. Shpyrko, H. L. Xin, N. Tamura, C. Tian and T.-C. Weng, *Chemical reviews*, 2017, **117**, 13123-13186.
31. L. Wang, J. Wang and P. Zuo, *Small Methods*, 2018, 1700293.
32. W. Huang, A. Marcelli and D. Xia, *Advanced Energy Materials*, 2017.
33. J. Wang, J. Zhou, Y. Hu and T. Regier, *Energy & Environmental Science*, 2013, **6**, 926-934.
34. J. Zhou, J. Wang, C. Sun, J. Maley, R. Sammynaiken, T. Sham and W. Pong, *Journal of Materials Chemistry*, 2011, **21**, 14622-14630.
35. A. Sakdinawat and D. Attwood, *Nature photonics*, 2010, **4**, 840.
36. K. Kaznatcheev, C. Karunakaran, U. Lanke, S. Urquhart, M. Obst and A. Hitchcock, *Nuclear Instruments and Methods in Physics Research Section A: Accelerators, Spectrometers, Detectors and Associated Equipment*, 2007, **582**, 96-99.
37. J. Kang, J. D. Wood, S. A. Wells, J.-H. Lee, X. Liu, K.-S. Chen and M. C. Hersam, *ACS nano*, 2015, **9**, 3596-3604.
38. Z. Guo, H. Zhang, S. Lu, Z. Wang, S. Tang, J. Shao, Z. Sun, H. Xie, H. Wang and X. F. Yu, *Advanced Functional Materials*, 2015, **25**, 6996-7002.
39. G. Nicotra, A. Politano, A. Mio, I. Deretzis, J. Hu, Z. Mao, J. Wei, A. La Magna and C. Spinella, *physica status solidi (b)*, 2016, **253**, 2509-2514.
40. J. Prietzel, J. Thieme and D. Paterson, *Journal of Plant Nutrition and Soil Science*, 2010, **173**, 805-807.
41. G. Küper, R. Chauvistré, J. Hormes, F. Frick, M. Jansen, B. Lüer and E. Hartmann, *Chemical physics*, 1992, **165**, 405-414.

42. E. D. Ingall, J. A. Brandes, J. M. Diaz, M. D. de Jonge, D. Paterson, I. McNulty, W. C. Elliott and P. Northrup, *Journal of synchrotron radiation*, 2011, **18**, 189-197.
43. B. Ravel and M. Newville, *Journal of synchrotron radiation*, 2005, **12**, 537-541.
44. G. Kresse and J. Furthmüller, *Physical review B*, 1996, **54**, 11169.
45. S. Grimme, J. Antony, S. Ehrlich and H. Krieg, *The Journal of chemical physics*, 2010, **132**, 154104.

Figures and Captions:

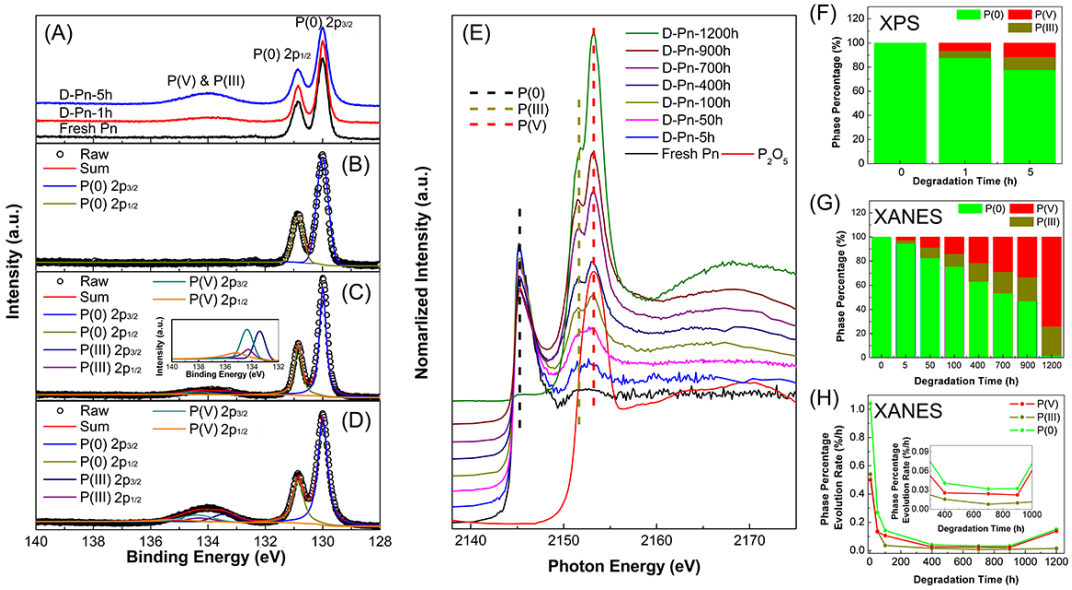

Figure 1 *In-situ* synchrotron-based XPS and XANES study of phosphorene degradation under ambient condition. (A) P 2p XPS spectra and (B~D) curve fitting result of fresh phosphorene and degraded phosphorene for 1, and 5 h. (E) Normalized XANES spectra of fresh phosphorene and degraded phosphorene for different time and the reference XANES spectra of P_2O_5. (F) Combination fitting result of *in-situ* XPS spectra. (G) Linear combination fitting result of *in-situ* XANES and (H) corresponding phase percentage evolution rate during *in-situ* XANES study process.

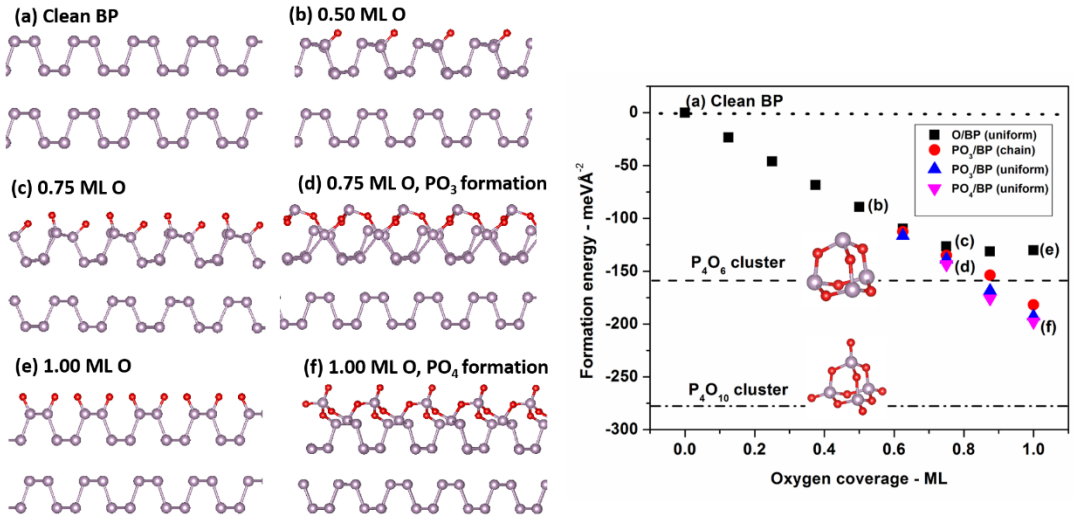

Figure 2 Calculated surface formation energies for various oxygen configurations on two-layer black phosphorene as a function of oxygen coverage. Energies are relative to clean phosphorene and compared to the formation energies of P_4O_6 and P_4O_{10} clusters in the gas phase.

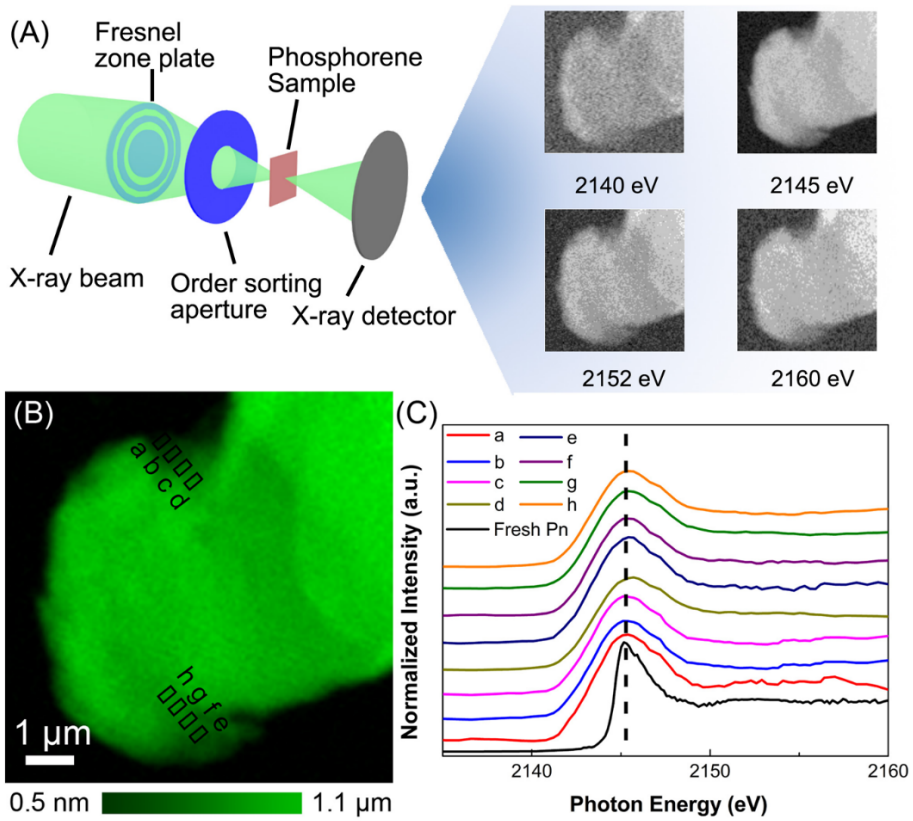

Figure 3 (A) Schematic illustration of the working principle of STXM at SM beamline, Canadian Light Source and X-ray microscopy images of fresh phosphorene at several photon energies; (B) Thickness map of fresh phosphorene derived from P K-edge. The horizontal bar in (B) illustrate the green scale representing the phosphorene thickness in nm. Based on the thickness distribution, several regions have been marked as a, b, c, d, e, f, g, and h, indicating the regions of interest. (C) Normalized XANES spectra of the regions marked in (B) at the P K-edge and fresh Pn.

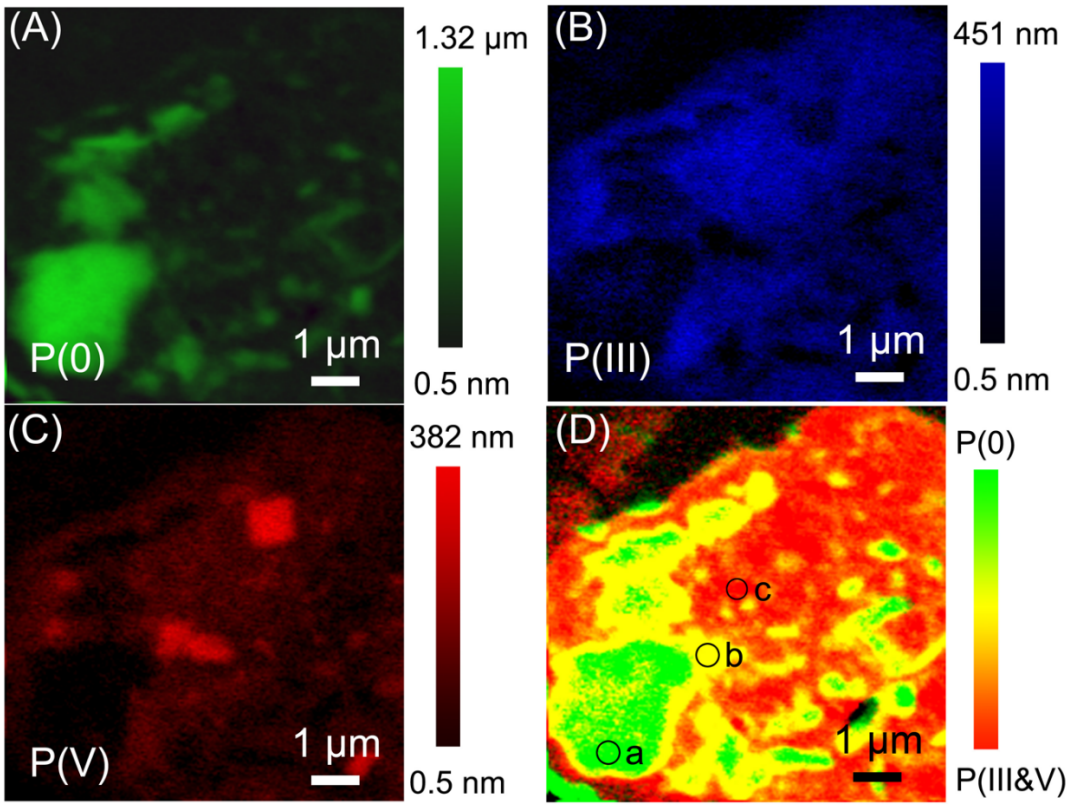

Figure 4 Thickness map derived from P K-edge of (A) P(0), (B) P(III), and (C) P(V) in D-Pn-30d. The vertical bars in (A), (B), (C) illustrate the green, blue, and red scale representing the thickness in nm. (D) Quasi-quantitative chemical phase map of D-Pn-30d (green: P(0), red: P(III&V). Three regions of interest have been marked as a, b, and c.

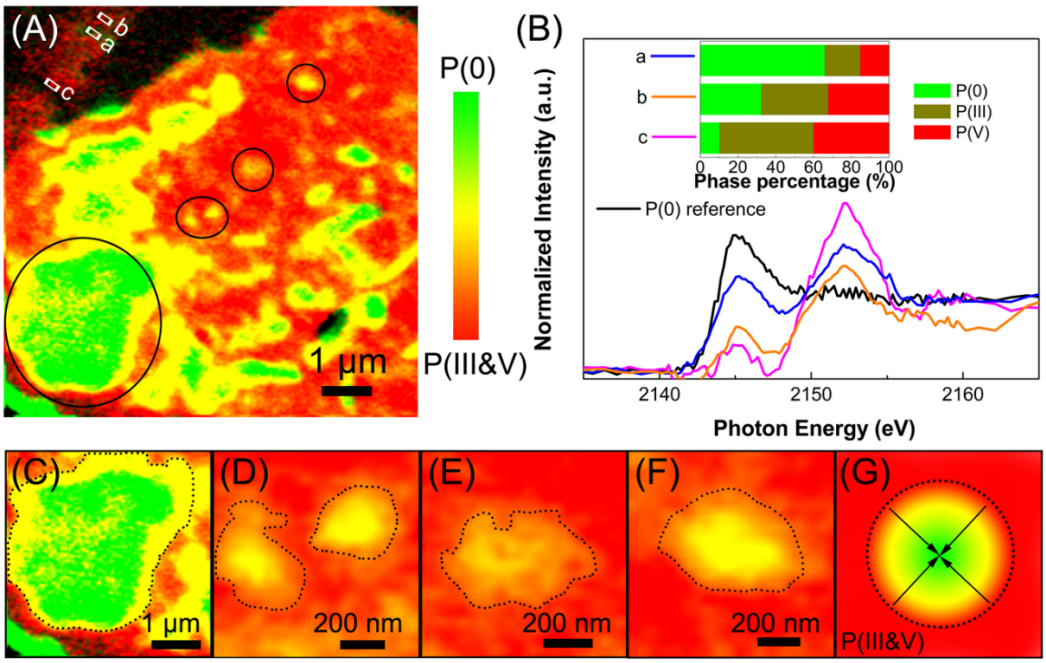

Figure 5 (A) Quasi-quantitative chemical phase map of D-Pn-30d (green: P(0), red: P(III&V)). Several ROIs have been selected to understand the morphology effect. Regions of interest a, b, and c have been selected to study the thickness effect and other four regions marked with black circles are used to study the neighborhood effect. (B) Normalized XANES spectra of the regions a, b, and c marked in (A), P^0, and P^{4+} with one insert of linear combination fitting result of each XANES spectrum. (C-F) Four regions have been marked black circles in (A) to understand the neighborhood effect and (G) Schematic illustration of the neighborhood effect.

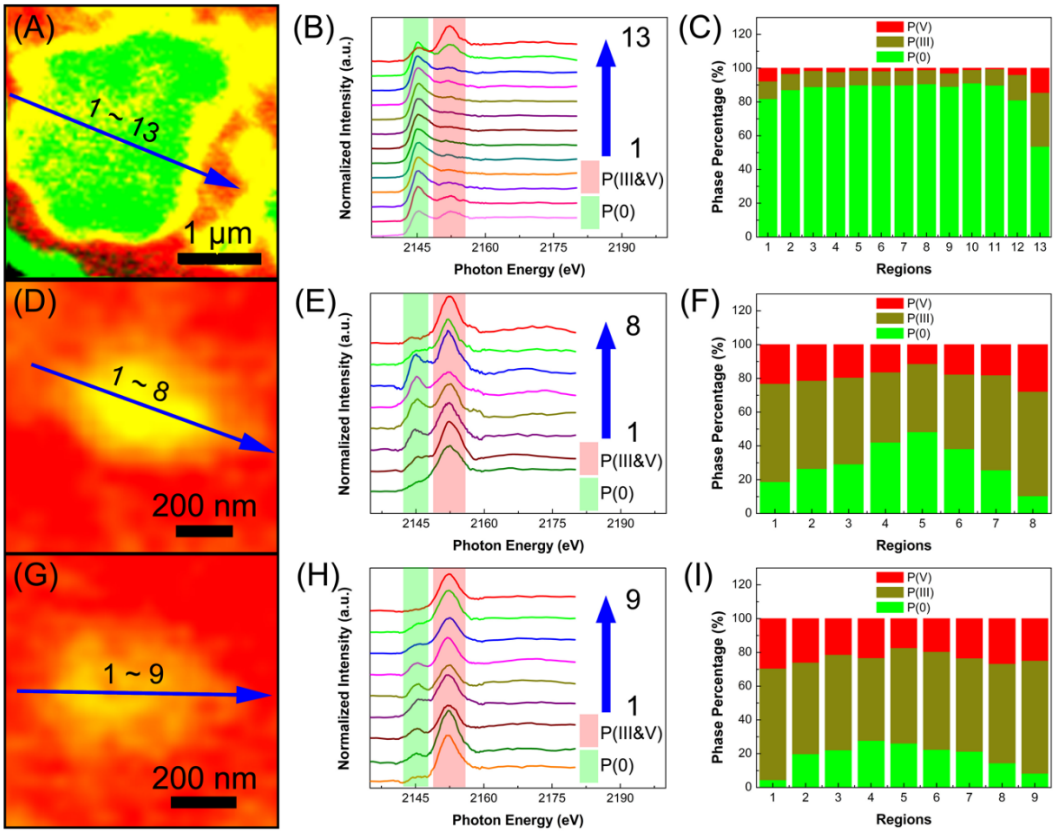

Figure 6 (A & D & G) Quasi-quantitative chemical phase map of several ROIs (green: P(0), red: P(III&V)). (B & E & H) Normalized XANES spectra and (C & F & I) Linear combination fitting result of several parts marked by blue arrows in (A & D & G).

TOC

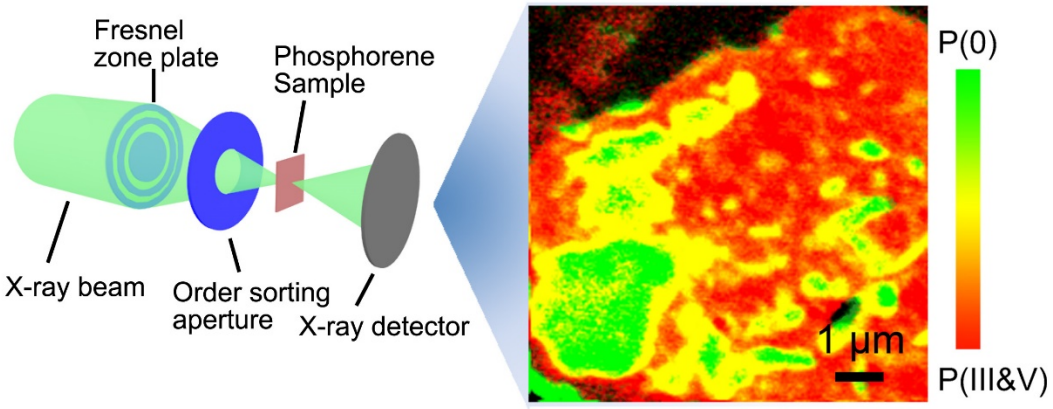

A clear nanoscale chemical imaging of the morphology effect during phosphorene degradation under ambient condition by conducting scanning transmission X-ray microscopy combined with *in-situ* synchrotron-based X-ray photoelectron spectroscopy and X-ray absorption fine structure study.

Supporting Information

Phosphorene Degradation: Visualization and Quantification of Nanoscale Phase Evolution by Scanning Transmission X-ray Microscopy

*Weihan Li[1, 2, #], Zhiqiang Wang [2, #], Feipeng Zhao[1, #], Minsi Li[1,2], Yang Zhao,[1] Xuejie Gao[1,2], Jian Wang,[3] Jigang Zhou,[3] Yongfeng Hu,[3] Qunfeng Xiao,[3] Xiaoyu Cui[3], Mohammad Javad Eslamibidgoli[4, †], Michael. H. Eikerling[4, †], Ruying Li [1], Frank Brandys[5], Ranjith Divigalpitiya[5], Tsun-Kong Sham [2, *], Xueliang Sun[1,*]*

[1]*Department of Mechanical and Materials Engineering, University of Western Ontario, London, Ontario, N6A 5B9, Canada*
[2] *Department of Chemistry and Soochow-Western Centre for Synchrotron Radiation Research, University of Western Ontario, London, Ontario, N6A 5B7, Canada*
[3] *Canadian Light Source, 44 Innovation Boulevard, Saskatoon, Saskatchewan, S7N 2V3, Canada*
[4] *Department of Chemistry, Simon Fraser University, 8888 University Drive, Burnaby, V5A 1S6, BC, Canada*
[5]*3M Canada Company, 1840 Oxford Street East, London, Ontario, N5V 3R6, Canada*

*Corresponding Author: Xueliang Sun, Tel: +1-519-661-2111 Ext 87759; Tsun-Kong Sham, Tel: Tel: +1-519-661-2111 Ext 86341;

E-mail address: xsun9@uwo.ca (X. Sun); tsham@uwo.ca (T.K. Sham)

[#]These authors contributed equally to this work.

[†] These authors contributed in the theoretical study of this work.

Experimental Sections

Materials Preparation method:

Phosphorene: Similar to the previous report,[1] phosphorene 45 mg of Bulk black phosphorus (purchased from Smart Elements) was immersed in 45 mL of N-Methyl-2-pyrrolidone (NMP). Then solution was then used for liquid exfoliation by tip-sonication (Qsconica Q700 sonicator) with the amplitude 80 for 1 h. Then the as-prepared

dispersions were centrifuged with the speed of 7000 rpm for 1h to get the top half of the dispersion to obtain the phosphorene. The concentration of obtained phosphorene solution is around 0.23 mg mL^{-1}.

Morphology Characterization:

The morphology of the samples was characterized by a Hitachi S-4800 field emission scanning electronic microscopy (FESEM) and a JEOL 2010F field emission TEM. Raman spectra was obtained using a HORIBA Scientific LabRAM HR Raman spectrometer system equipped with a 532.4 nm laser. Atomic force microscopy (AFM) measurement was performed by means of the Park Systems XE-100 system.

X-ray photoelectron spectroscopy & X-ray absorption near-edge spectroscopy

The P 2p XPS spectra of phosphorene during degradation process under ambient condition were collected at Variable line spacing plane grating monochromator (VLS-PGM) beamline. XPS measurements were performed immediately at a base pressure of ~ 10^{-9} mbar. The excitation photon energy was set at 240 eV. The P K-edge XANES spectra of phosphorene and reference samples, including bulk black phosphorus and P_2O_5 were collected at the Soft X-ray Microcharacterization Beamline (SXRMB) at the Canadian Light Source. One detection mode was used for the XANES spectra,, fluorescence yield (FLY) mode. For the *in-situ* XPS and XANES study of the phosphorene degradation process, the samples were degraded for different time and the P 2p XPS and K-edge XANES spectra were acquired by focusing the beam at the same position.

Scanning transmission X-ray microscopy

STXM measurement was conducted at the SM beamline of the Canadian Light Source (CLS), which is equipped with a 25 nm outermost-zone zone plate (CXRO, Berkeley Lab).[2] The diffraction limited spatial resolution for this zone plate is 30 nm. The phosphorene samples were raster-scanned with synchronized detection of transmitted

X-rays to generate images. Chemical imaging and XANES spectra are obtained using image sequence (stack) scans over a range of photon energies at the P K-edge. STXM data was analyzed using the aXis2000 software package (http://unicorn.mcmaster.ca/aXis2000.html), which allows for detailed interactive processing of the images and fitting of the X-ray absorption spectra. XANES from interesting locations were extracted from image stacks using image mask which only selects the regions of interest. XANES from fresh phosphorene and fully oxidized regions were used as reference spectra for stack fitting to generate chemical component maps. The color composite map was created by combining individual component maps with the image intensity rescaled for better visualization.

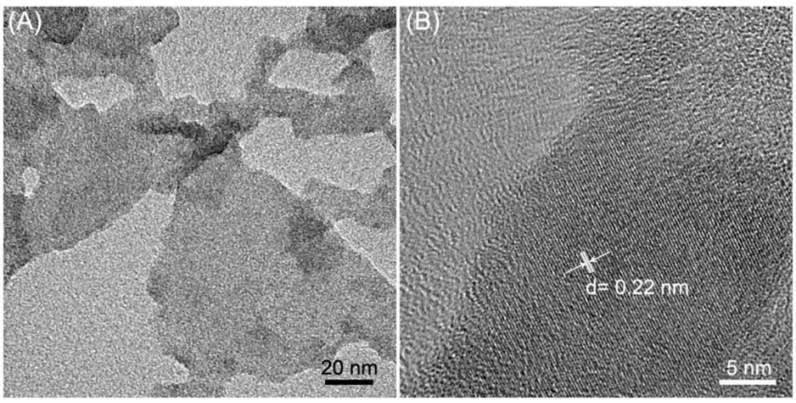

Figure S1 (A) TEM and (B) HRTEM images of fresh phosphorene nanosheets.

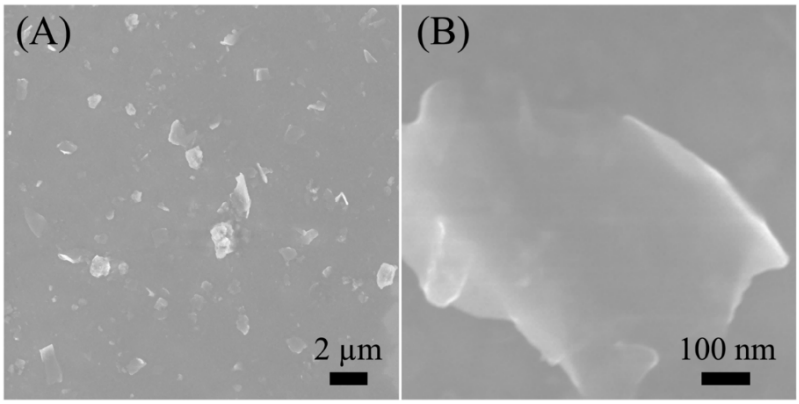

Figure S2 SEM image of phosphorene nanosheets

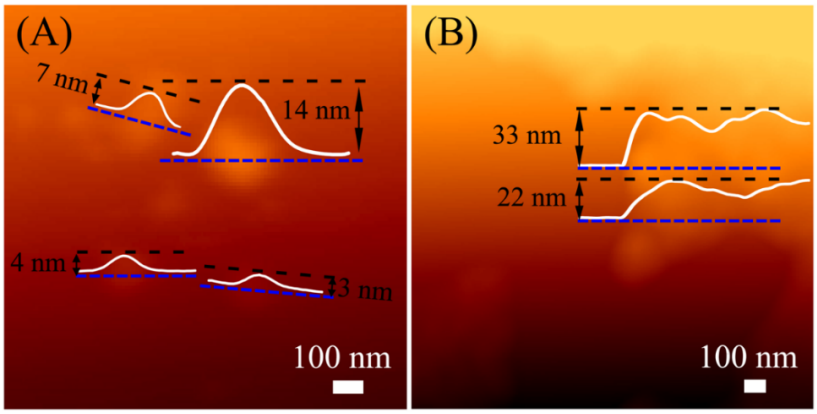

Figure S3 AFM images of fresh phosphorene nanosheets (A) and phosphorene degraded under ambient condition for 30d (B).

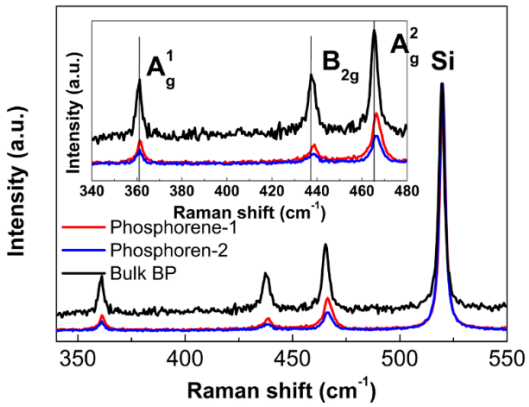

Figure S4 Raman spectra of phosphorene and bulk BP, which are deposited on the SiO2/Si substrates. Compared with the bulk BP, the phosphorene shows the blue-shift of Raman peaks and reduction of the intensity ration between BP and Si peaks.

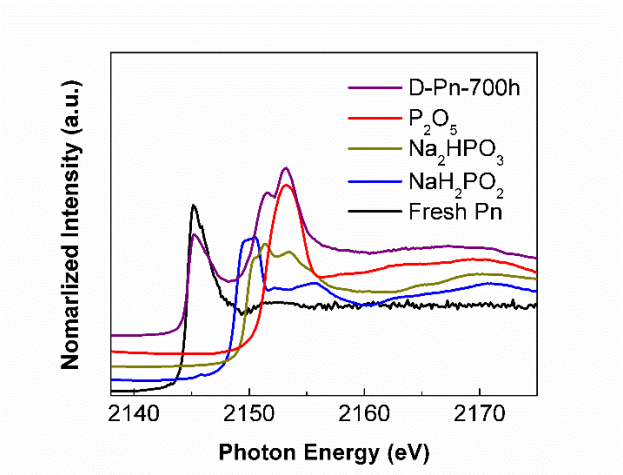

Figure S5 Normalized XANES spectra of fresh phosphorene and D-Pn-700h acquired form the *in-situ* XANES study and the reference XANES spectra of NaH_2PO_2 (i.e. P(I)), Na_2HPO_3 (i.e. P(III)), and P_2O_5 (i.e. P(V)).

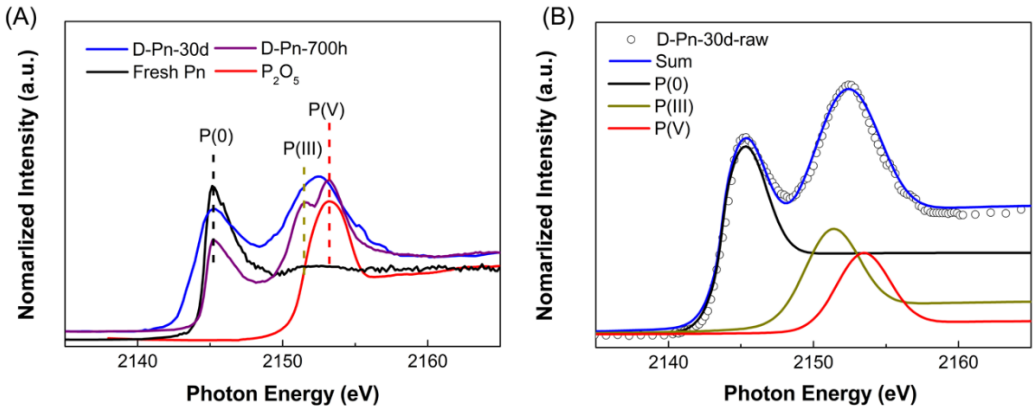

Figure S6 (A) Normalized XANES spectra of D-Pn-30d, fresh phosphorene and D-Pn-700h acquired form the *in-situ* XANES study and the reference XANES spectra of P_2O_5. (B) Normalized XANES fitting result of D-Pn-30d based P(0), P(III), and P(V) components. Based on calculation, phase percentage of P(0), P(III), and P(V) is 6:3:1.

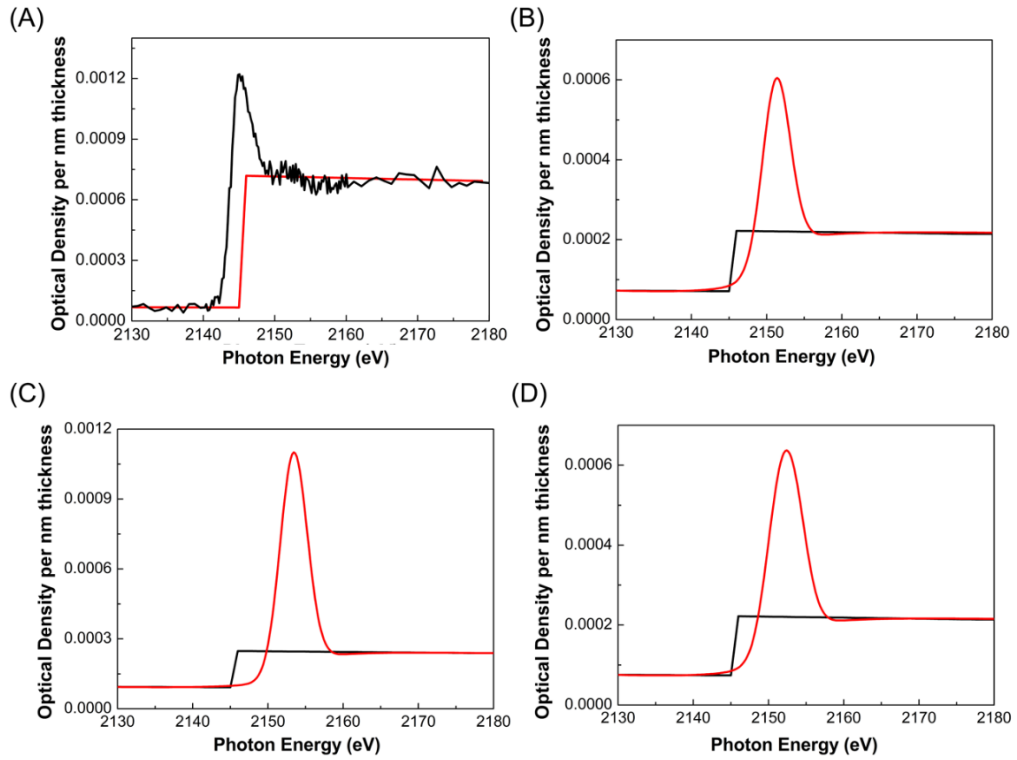

Figure S7 Reference spectra and elemental linear X-ray absorption profiles of (A) fresh phosphorene, (B) H_3PO_3, (C) H_3PO_4 and (D) mixed phosphoric acid (3/4 H_3PO_3+1/4 H_3PO_4) at P K-edge (black line: optical density spectrum of 1 nm thickness, red line: elemental linear X-ray absorption profile based on formula P (density = 2.69 g/cm^3), H_3PO_3 (density = 1.65 g/cm^3), H_3PO_4 (density = 1.88 g/cm^3) and mixed phosphoric acid (density = 1.708 g/cm^3) and thickness = 1 nm.)[3,4] The reference spectrum of fresh phosphorene is acquired from the regions displaying single P(0) peaks. In the case of phosphoric acid, the reference spectra are acquired based on XANES fitting of overall XANES of D-Pn-30d.

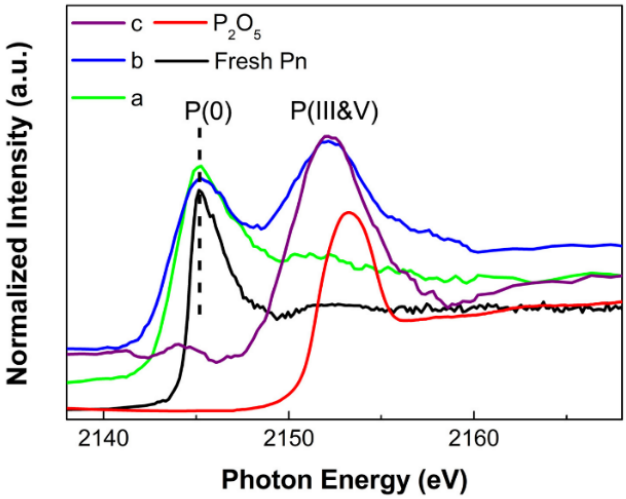

Figure S8 Normalized XANES spectra of the regions (i.e. a, b, and c) marked in Figure 4D, fresh-Pn and P_2O_5 at the P K-edge.

Table S1 Thickness information of P(0), P(III), and P(V) in the marked regions in Figure 5A.

Region	Thickness of P(0) / nm	Thickness of P(III) / nm	Thickness of P(V) / nm	Thickness of overall phosphorene before degradation / nm *
a	8.4	3.9	2.8	9.8
b	4.9	8.8	7.0	8.5
c	1.2	9.2	6.5	4.7

* The thickness of phosphorene before degradation is calculated based on the thickness of P(0), P(III), and P(V) in the regions of D-Pn-30d. Assuming that the phosphoric acid is formed from the phosphorene at the same position, the thickness of phosphorene corresponding to phosphoric acid can be calculated based on the density of phosphorene (density = 2.69 g/cm^3), H_3PO_3 (density = 1.65 g/cm^3), and H_3PO_4 (density = 1.88 g/cm^3).

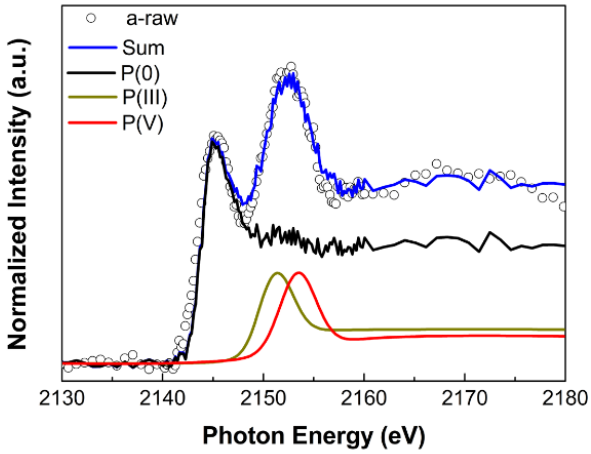

Figure S9 Linear combination fitting (LCF) analysis of the XANES spectrum of region a in the Figure 5A & 5B.

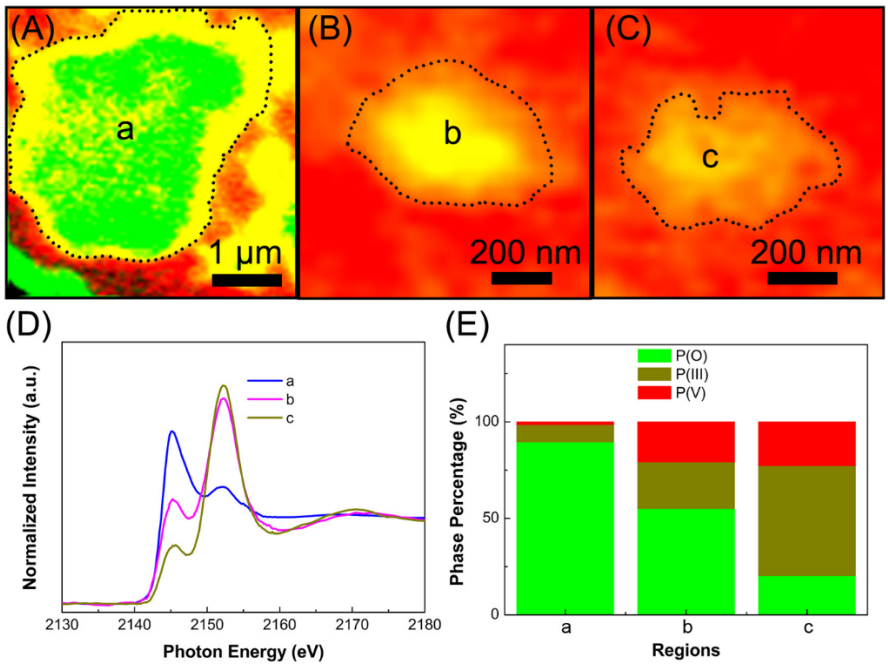

Figure S10 (A~C) Quasi-quantitative chemical phase map of several ROIs (green: P(0), red: P(III&V)) marked in Figure 5. (D) Normalized XANES spectra and (E) Linear combination fitting result of overall regions marked by dash lines in (A~C).

Theoretical Section

Coordinates of the main structures studied in this work:

P_4O_6 Cluster

1.00000000000000

20.0000000000000000 0.0000000000000000 0.0000000000000000

0.0000000000000000 20.0000000000000000 0.0000000000000000
0.0000000000000000 0.0000000000000000 20.0000000000000000
P O
4 6
Selective dynamics
Direct
0.4231623266033631 0.5001481024479418 0.5005291061100284 T T T
0.5445728734750768 0.5425258120347787 0.5736439371766628 T T T
0.5432091750382704 0.5422391101246823 0.4249022581859703 T T T
0.5433540382962964 0.4135519071409670 0.4995973371203647 T T T
0.4606324334334432 0.4259476123957664 0.5004220058871461 T T T
0.5640681081706527 0.4622593426966967 0.4353853961628717 T T T
0.5652817602062139 0.4626415736002390 0.5631885732974505 T T T
0.5651449046683289 0.5732223477142775 0.4991457147659510 T T T
0.4605004876535506 0.5368787067485921 0.4362163057014964 T T T
0.4617970160701414 0.5371003705323636 0.5641896356716666 T T T

P_4O_{10} Cluster
1.00000000000000
20.0000000000000000 0.0000000000000000 0.0000000000000000
0.0000000000000000 20.0000000000000000 0.0000000000000000
0.0000000000000000 0.0000000000000000 20.0000000000000000
P O
4 10
Selective dynamics
Direct
0.4258446293922518 0.4999371973984807 0.5006584001847543 T T T
0.5432397546524186 0.5409083602037299 0.5706982998470309 T T T
0.5417500134519386 0.5406207821988289 0.4279658241674653 T T T
0.5420522324919688 0.4171143561379438 0.4995638042981270 T T T
0.5660520086056522 0.3488653023704771 0.4994379259899020 T T T
0.4613978238546963 0.4268889674846861 0.5004018289247156 T T T
0.5638286379030504 0.4628892455087410 0.4361623897520985 T T T
0.5651533099465027 0.4631521655851500 0.5623121084468181 T T T
0.5655151052610137 0.5744186443879400 0.3685859269128073 T T T
0.5648489919282014 0.5723949542413607 0.4990291044262847 T T T
0.4611572470939365 0.5362044026617667 0.4371184266981558 T T T
0.5682638370059365 0.5749481470119591 0.6294215830145617 T T T
0.4624504829003726 0.5364044540156172 0.5633100833341658 T T T
0.3535135100027702 0.5001083075337363 0.5013269273542491 T T T

2-layer black phosphorus slab

1.00000000000000

6.5933566099999998 0.0000000000000000 0.0000000000000000

0.0000000000000000 35.0000000000000000 0.0000000000000000

0.0000000000000000 0.0000000000000000 8.7565517400000008

P

32

Selective dynamics

Direct

0.8749547386893665	0.3941656070037122	0.9595157399697710	T	T	T
0.6250425625822617	0.3941150240480835	0.7904146089071066	T	T	T
0.3750356773553244	0.3941269944615804	0.9594670189739617	T	T	T
0.1249694607056347	0.3941361330578123	0.7904639394661853	T	T	T
0.8750633505069824	0.3941543921763538	0.4594829730497019	T	T	T
0.6250202563582418	0.3941331676722745	0.2904527207653067	T	T	T
0.3749623563667544	0.3941104284557225	0.4594619651694699	T	T	T
0.1249839213630310	0.3941372656104080	0.2903847176516108	T	T	T
0.8751923473201166	0.4553376820984282	0.5400239944024726	T	T	T
0.6251356617651527	0.4552942739749137	0.7094944441873489	T	T	T
0.3750505273279697	0.4552924695598898	0.5400951920682222	T	T	T
0.1251100753204211	0.4553171854048272	0.7096738455178371	T	T	T
0.8747906475458820	0.4553537985586797	0.0401302726895862	T	T	T
0.6248847652610626	0.4553240712384783	0.2097836308464359	T	T	T
0.3750350818268400	0.4553127989709020	0.0401135049042596	T	T	T
0.1249382962135879	0.4553238763976035	0.2095444643469861	T	T	T
0.8750001506627595	0.5503829735750465	0.7902479461057057	T	T	T
0.6249987838301515	0.5503833983524391	0.9597437864244049	T	T	T
0.3750011423520169	0.5503829908555257	0.7902472448985742	T	T	T
0.1250015595774350	0.5503836252403344	0.9597436059438565	T	T	T
0.8749999870855641	0.5503831967299823	0.2902474899043508	T	T	T
0.6249994901190931	0.5503833835345179	0.4597436675815139	T	T	T
0.3750009012942552	0.5503831073227070	0.2902469184795998	T	T	T
0.1250023385243166	0.5503829989183905	0.4597431211396072	T	T	T
0.8750008389271130	0.6115751307552323	0.7095274058725718	T	T	T
0.6250004930798388	0.6115750518029706	0.5404679032934465	T	T	T
0.3749999321195537	0.6115753168882738	0.7095272935977266	T	T	T
0.1250002864283467	0.6115751121396413	0.5404669775474672	T	T	T
0.8750003997294957	0.6115752152250253	0.2095268383511459	T	T	T
0.6250006374716943	0.6115754237633929	0.0404669492931279	T	T	T
0.3750010064024901	0.6115754574544816	0.2095268709818766	T	T	T
0.1250007333644753	0.6115752273155374	0.0404675460125559	T	T	T

2-layer black phosphorus / 1 monolayer O^{ad}

1.00000000000000

6.5933566099999998 0.0000000000000000 0.0000000000000000

0.0000000000000000 35.0000000000000000 0.0000000000000000
0.0000000000000000 0.0000000000000000 8.7565517400000008
P O
32 8
Selective dynamics
Direct
0.8749489530740211 0.3942250133061065 0.9596309499621288 T T T
0.6250467534677692 0.3941749768520301 0.7902720394418901 T T T
0.3750411494305936 0.3941901053263898 0.9595851612758534 T T T
0.1249660458114242 0.3941946816819162 0.7903461428557713 T T T
0.8750701699870933 0.3942131122684992 0.4595943524969884 T T T
0.6250230488591563 0.3941911866929003 0.2903315946118232 T T T
0.3749564968886774 0.3941653993390605 0.4595509555384553 T T T
0.1249811769529839 0.3941945025072678 0.2902529128821565 T T T
0.8751702694128741 0.4552883638588525 0.5400912882687648 T T T
0.6251386466484085 0.4552486564998194 0.7094691728157181 T T T
0.3750382002303633 0.4552525679158826 0.5401456889257533 T T T
0.1251055695560736 0.4552733595916408 0.7096320810144309 T T T
0.8748161154979845 0.4553033593526216 0.0401873488461758 T T T
0.6248924025735101 0.4552778535111827 0.2097363649975786 T T T
0.3750365087436500 0.4552708957214648 0.0401638167321045 T T T
0.1249357925930311 0.4552716224889805 0.2095017491730232 T T T
0.8749994330981261 0.5519822770792185 0.7902349860882701 T T T
0.6249991734002258 0.5519829331699878 0.9597601647709039 T T T
0.3750008366511193 0.5519822647842264 0.7902338742785485 T T T
0.1250007995594055 0.5519829383058050 0.9597586441708635 T T T
0.8750003252996505 0.5519825151764201 0.2902350011747855 T T T
0.6249991493025611 0.5519826153611868 0.4597588693885104 T T T
0.3749999530882078 0.5519825191520817 0.2902334333494432 T T T
0.1250013663235537 0.5519824014405623 0.4597593349195159 T T T
0.8750038315420268 0.6119474545579101 0.7038598368256707 T T T
0.6249989940113313 0.6119480679431887 0.5461402302445499 T T T
0.3749993828031196 0.6119471666460083 0.7038616444834542 T T T
0.1250041302356675 0.6119476434047514 0.5461377156414151 T T T
0.8749990405087930 0.6119479695039153 0.2038578591258582 T T T
0.6249959508010131 0.6119477694977015 0.0461362301501825 T T T
0.3750045810123367 0.6119476980440146 0.2038605272170496 T T T
0.1250046730909578 0.6119478053177489 0.0461388485839309 T T T
0.8750001232054972 0.6506435827499509 0.2710107661985482 T T T
0.3749999494125396 0.6506438808644436 0.2710101847373390 T T T
0.6250001266726340 0.6506432594632885 0.4789856318632341 T T T
0.1249998921833354 0.6506434470526231 0.4789860621370583 T T T
0.8749998433905697 0.6506435988450732 0.7710106150410165 T T T
0.3749999040751440 0.6506438561025650 0.7710102024976816 T T T

0.6249999068936120 0.6506437211861114 0.9789864561490512 T T T
0.1249997411881870 0.6506433326184050 0.9789858640363341 T T T

2-layer black phosphorus / 0.75 monolayer O^{ad} (precursor for P_4O_6 formation)

1.00000000000000
6.5933566099999998 0.0000000000000000 0.0000000000000000
0.0000000000000000 35.0000000000000000 0.0000000000000000
0.0000000000000000 0.0000000000000000 8.7565517400000008
P O
32 6
Selective dynamics
Direct
0.8749999994312461 0.3941499591428581 0.9599851367976981 T T T
0.6249999998104130 0.3941499591428581 0.7900148637733082 T T T
0.3750000001895870 0.3941499591428581 0.9599851367976981 T T T
0.1250000005687539 0.3941499591428581 0.7900148637733082 T T T
0.8749999994312461 0.3941499591428581 0.4599851367976981 T T T
0.6249999998104130 0.3941499591428581 0.2900148626313026 T T T
0.3750000001895870 0.3941499591428581 0.4599851367976981 T T T
0.1250000005687539 0.3941499591428581 0.2900148626313026 T T T
0.8754523812164668 0.4553610911464935 0.5398818751067738 T T T
0.6250454854552325 0.4552936561335155 0.7093777346256663 T T T
0.3750591766200425 0.4552522669753424 0.5400181262236956 T T T
0.1250798624113633 0.4552798603183699 0.7099143317425028 T T T
0.8746641408699459 0.4553702353597420 0.0399376153733402 T T T
0.6250118296968208 0.4552845506846497 0.2099559464230878 T T T
0.3750505085215845 0.4552696182947223 0.0400442337394883 T T T
0.1250495648602466 0.4552941438818569 0.2094304409192846 T T T
0.8378974905893146 0.5527535015934318 0.7506097977386310 T T T
0.5921540027203314 0.5490747834964224 0.9182995096293802 T T T
0.3333717131802618 0.5575613538339402 0.7619806562984239 T T T
0.0731268255877908 0.5540919398286012 0.9235053790725948 T T T
0.9204785386876204 0.5528903432560508 0.2500399484297598 T T T
0.6849324550138000 0.5534128405204106 0.4228739910841640 T T T
0.4256013978815967 0.5575777829598056 0.2602641417520280 T T T
0.1674578867276365 0.5487541823438148 0.4165920531765839 T T T
0.8450460538185547 0.6651559245136891 0.8524822161447357 T T T
0.7540385999222697 0.6073642417824903 0.5811835770476890 T T T
0.3844074365869242 0.6163186966741420 0.6782595925567831 T T T
0.1242401464059616 0.6047270573690150 0.5289470482348558 T T T
0.9132460539603348 0.6648224359182834 0.3547173187229423 T T T
0.6349872958063320 0.6053637306751670 0.0285800076680810 T T T
0.3763246862232741 0.6166215053349692 0.1790752349195394 T T T

0.0016772101234707 0.6080310646076938 0.0811828558308247 T T T
0.9348154467948072 0.6507462886929608 0.1821680083585120 T T T
0.7391593940977197 0.6355242118454912 0.4231372205659689 T T T
0.1250256983161002 0.6433440640318736 0.4250439655654411 T T T
0.8233291639329938 0.6502011392965507 0.6811108660213924 T T T
0.6333962455873700 0.6439953411742491 0.9248808188753220 T T T
0.0194263179016993 0.6364077156734391 0.9237953449191554 T T T

Monolayer black phosphorus / 1.0 monolayer O^{ad} (precursor for P_4O_{10} formation)

1.00000000000000

6.5933566099999998 0.0000000000000000 0.0000000000000000
0.0000000000000000 35.0000000000000000 0.0000000000000000
0.0000000000000000 0.0000000000000000 8.7565517400000008

P O
16 8
Selective dynamics
Direct
0.8618452625779298 0.5399288814313152 0.8405517848333162 T T T
0.6103862354928680 0.5505236396660607 0.0000289490105985 T T T
0.3463249079624688 0.5480004155103160 0.8356591924713541 T T T
0.0905587447761533 0.5520998457118012 0.0002839968754031 T T T
0.8798277453395258 0.5532581185878129 0.3046499382022176 T T T
0.6440987248141425 0.5405015897374668 0.4580798030785616 T T T
0.3915306898155180 0.5497581340158533 0.3006496325859445 T T T
0.1351147224016742 0.5458526078528294 0.4705545545903362 T T T
0.8303523965475748 0.6151345185816481 0.6418739231846828 T T T
0.7022078903126285 0.6641418439874016 0.3911977639933681 T T T
0.3703522593759061 0.6077625537291240 0.7390696292090482 T T T
0.1491328095842945 0.6072860026940177 0.5410063191357892 T T T
0.9260362198883669 0.6188730780795169 0.1498407963920485 T T T
0.6092596645260002 0.6129875603737389 0.0465256825491096 T T T
0.3869032721868351 0.6129947268396378 0.2461217880955573 T T T
0.0530583455790534 0.6623341441486517 0.8751409413049487 T T T
0.8909148677486840 0.6455491613918269 0.3021046653963992 T T T
0.5324136718404446 0.6312603967409416 0.3836464464824232 T T T
0.7761254510019526 0.6578942186768018 0.5618700150761029 T T T
0.8808701162928116 0.6341159409575710 0.8078622059003777 T T T
0.2541229805263754 0.6367672731831178 0.8618887000274427 T T T
0.9996030575947117 0.6587349472972051 0.0504180941265560 T T T
0.6417766534801430 0.7025787812168289 0.3471118969417049 T T T
0.0667740911062253 0.7007682133028013 0.8123774230683480 T T T

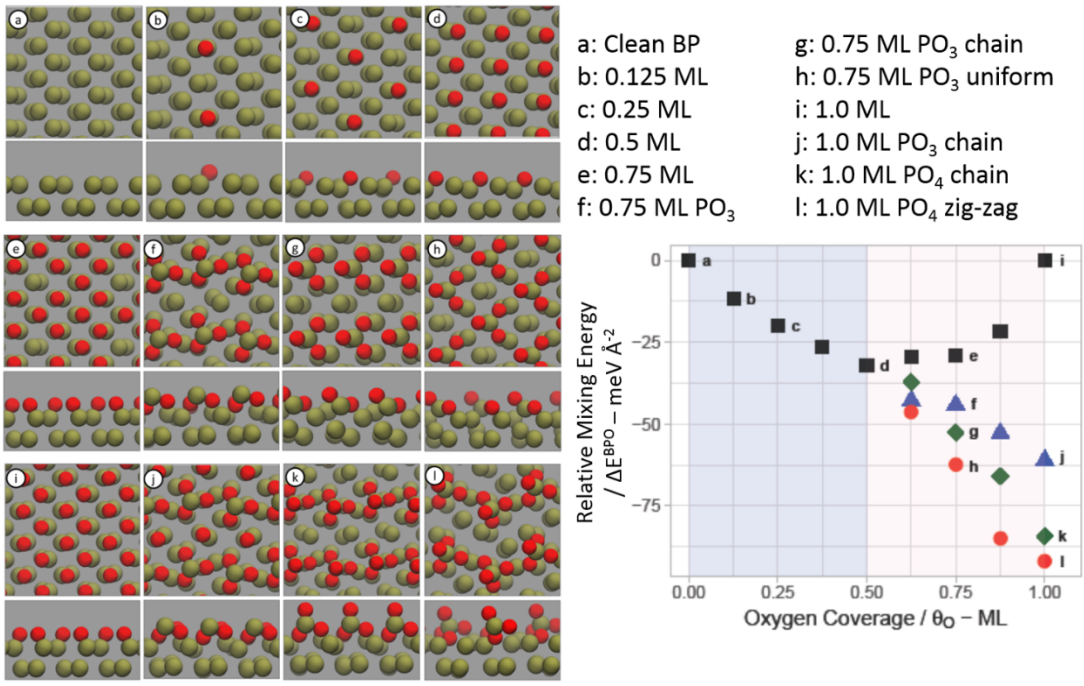

Figure S11. Calculated surface mixing energies for various oxygen configurations on phosphorene as a function of oxygen coverage. Adopted from ref. 5.

References:

1. J. Kang, J. D. Wood, S. A. Wells, J.-H. Lee, X. Liu, K.-S. Chen and M. C. Hersam, *ACS nano*, 2015, **9**, 3596-3604.
2. J. Wang, J. Zhou, Y. Hu and T. Regier, *Energy & Environmental Science*, 2013, **6**, 926-934
3. H. Liu, Y. Du, Y. Deng and D. Y. Peide, *Chemical Society Reviews*, 2015, **44**, 2732-2743.
4. A. D. Toy, *The Chemistry of Phosphorus: Pergamon Texts in Inorganic Chemistry*, Elsevier, 2016.
5. M. J. Eslamibidgoli, M. H. Eikerling, *The Journal of Physical Chemistry C* 122.39 (2018): 22366-22373.